Noname manuscript No.
(will be inserted by the editor)

Eliminating synchronization in bistable networks

Irmantas Ratas and Kestutis Pyragas

Received: date / Accepted: date

Abstract The problem of controlling synchrony in bistable networks, which possess coherent and incoherent attractors in a certain range of parameters, is considered. Along with the known Kuramoto-type models, we introduce the bistable networks consisting of all-to-all coupled noisy FitzHugh-Nagumo neurons as well as chaotic Rulkov neurons. We suggest two different algorithms to switch the bistable networks from the stable coherent state to the stable incoherent state. One of them is an act-and-wait control method, which utilizes the mean field measurements and homogeneous time delayed feedback perturbations with the periodically switched on and off feedback gain. We show that this algorithm is efficient for the globally coupled populations. Another algorithm is based on the multisite coordinated reset stimulation. The algorithm is nonfeedback, but it uses inhomogeneous perturbations and is efficient even for the networks with a complex scale-free topology. In addition to the numerical analysis of finite size networks, the analytical results for the Kuramoto-type models in the thermodynamic limit are presented.

Keywords Complex networks · Synchronization · Neuron models · Control of bistability

1 Introduction

Systems of many interacting oscillatory elements are of great interest in a wide variety of scientific fields including physics, chemistry, and biology [1–4]. Synchronous behavior appearing in such systems may be useful for practical applications, e.g. for generation of strong coherent fields in coupled arrays of lasers or Josephson junctions. However, in many cases the synchronization is undesired and should be suppressed. An example of a dangerous synchronization is the lateral swing of London's Millennium Bridge caused by coherent motion of walkers [5].

The observations of synchronous neural activity in the central nervous system have stimulated a great deal of theoretical work on synchronization in neural networks [6]. The synchronization of oscillations is a mechanism for neural communication, which endows individual brain areas with the ability to perform specific tasks [7]. Conversely, extremely strong synchronization may impair brain function and cause various neurological disorders like Parkinson's disease [8–10] or epilepsy [11]. For this reason the research on control of synchronization in neural networks has attracted a great attention.

Methods for controlling synchronization in networks of coupled oscillators developed to date can be divided in two categories: (i) an open loop (nonfeedback) control and (ii) a closed loop (feedback) control. Nonfeedback algorithms are mainly based on a phase resetting stimulation [12–14]. The closed loop control methods are more diversified; they include linear [15–20] and nonlinear [21–23] time-delayed feedback control algorithms as well as other approaches [24–28]. All these algorithms have been developed to networks, which possess a stable coherent state and an unstable incoherent state. The aim of the algorithms was to stabilize an unstable incoherent state.

In this paper, we consider the problem of controlling synchrony in bistable networks, which possess the coexisting coherent and incoherent states, both being stable for the same values of the parameters. The specific asymptotic state of such a system depends on the initial conditions. The control problem that we formulate here is as follows. We assume that a bistable network is

I. Ratas (✉) · K. Pyragas Center for Physical Sciences and Technology, A. Goštauto 11, LT-01108 Vilnius, Lithuania
E-mail: irmantas.ff.vu@gmail.com

initially in the stable coherent state and our aim is to design a particular time-dependent perturbation which enables us to switch the system to the stable incoherent state. Such a problem can be motivated, e.g., by a possible control of epilepsy, which is modeled by a bistable neural network in which the disease and healthy states are associated with the stable coherent and incoherent states, respectively [11].

Generally, the control of multistable systems represents a rather complicated problem (see recent review [29] and references therein). There are no universal algorithms to solve this problem, since one has to deal with the global properties of the phase space of the controlled system. In our case, the control problem is especially difficult, since we employ rather hard constraints, which are typical for real-world neural networks. We assume that the individual oscillators of the network are not available for the separate control and measurements. The control is available only on the macroscopic level and we can measure only the mean field of the system. In this paper, we describe two strategies for controlling synchronization in bistable networks. The first strategy is based on an act-and-wait control algorithm [20,30–33], which represents a time delayed feedback control with a periodically switched on and off control gain. The second strategy utilizes a nonfeedback multisite coordinated reset (MCR) stimulation algorithm [13,14].

Synchronization bistability has been observed in different models of oscillatory networks. Most of them represent Kuramoto-type models in which individual oscillators are described by a phase variable. The coexisting stable coherent and incoherent states have been detected in networks of all-to-all coupled phase oscillators [34–38] as well as phase oscillators coupled via scale-free topology [39,40]. In the latter case only few oscillators have many links, while majority of them are attached to several oscillators. The synchronization bistability has been also analyzed in networks consisting of more complex elements such as FitzHugh-Nagumo (FHN) neurons [41] or chaotic oscillators [42].

We demonstrate our control algorithms for several models of bistable networks. First, we verify our control ideas on a generalized Kuramoto model [37], which admits an analytical treatment. Here the network consists of two types of phase oscillators, which are either positively (excitatory) or negatively (inhibitory) coupled to all other oscillators of the network. In addition, we introduce two bistable networks, constructing in analogy to Ref. [37], but instead of phase oscillators as units of the network, we utilize the FitzHugh-Nagumo [43,44] and Rulkov [45] neurons. Finally, we employ a network of phase oscillators connected via a scale-free topology [39].

The paper is organized as follows. In Sec. 2, four models of bistable networks are presented and the existence of a hysteresis in synchronization diagrams is demonstrated. Sections 3 and 4 are devoted to the act-and-wait and MCR control algorithms, respectively. Using numerical and analytical methods we demonstrate their capability to eliminate synchronization in the above described networks. The conclusions are presented in Sec. 5.

2 Models of bistable oscillatory networks

In this section, we briefly present four models of bistable oscillatory networks, which will be utilized as testing benchmarks for our proposed synchronization control algorithms (see Secs. 3 and 4). The models include networks of phase oscillators connected in all-to-all and scale-free topologies as well as networks of FHN and Rulkov neurons. For all these models, we demonstrate the synchronization bistability with the coexisting stable coherent and incoherent states. To this end, we compute a synchronization criterion as a function of a control parameter using forward and backward continuations and show that there is a hysteresis in this dependence.

2.1 Kuramoto model with positive and negative couplings

A generalized Kuramoto model that demonstrates synchronization bistability has been proposed in Ref. [37]:

$$\dot{\theta}_j = \omega_j + \frac{K_j}{N}\sum_{l=1}^{N}\sin(\theta_l - \theta_j), \quad j = 1,\dots,N. \tag{1}$$

Here θ_j is the phase of the jth oscillator and ω_j is its natural frequency, chosen at random from a unimodal, symmetric probability density $g(\omega)$. There are two types of oscillators in the population referred to as conformists and contrarians. The conformists are positively connected ($K_j > 0$) to all other oscillators of the population and they tend to fall in line with whatever rhythm has emerged in the population. The contrarians have negative coupling strength $K_j < 0$ and they are repelled by the prevailing rhythm. In terms of neuroscience, the positive and negative values of the coefficients K_j correspond to the excitatory a inhibitory coupling, respectively.

For the Kuramoto-type models, the collective rhythm is usually quantified by the complex order parameter

$$R = \frac{1}{N}\sum_{l=1}^{N} e^{i\theta_l}. \tag{2}$$

The absolute value $0 \le |R| \le 1$ of this parameter measures the macroscopic coherence of the system. The value $|R| = 0$ indicates the incoherent state while $|R| = 1$ defines the fully synchronized state. The values in-between represent partially synchronized states. By means of the definition (2), the system (1) can be rewritten as

$$\dot{\theta}_j = \omega_j + \mathrm{Im}\left[K_j R e^{-i\theta_j}\right], \quad j = 1, \ldots, N. \tag{3}$$

In our numerical simulations, we choose the natural frequencies of the oscillators from the Lorentz distribution

$$g(\omega) = (\Delta/\pi)\left[(\omega - \omega_0)^2 + \Delta^2\right]^{-1} \tag{4}$$

and then subdivide randomly the whole population of N oscillators into two groups with N_- and N_+ oscillators in each subpopulation. For all oscillators in the first subpopulation we assign the same negative value of the coupling strength $K_j = \kappa_1 < 0$ and label these oscillators as contrarians. Similarly, for the second, conformist subpopulation, we set $K_j = \kappa_2 > 0$. We also introduce the parameter $p = N_+/N$ that denotes the proportion of conformists in the population.

In Fig. 1, we present an example of a synchronization diagram that demonstrates the hysteresis in the dependence $|R|$ versus p and thus the existence of the bistability. The system (1) consisting of $N = 10000$ phase oscillators was numerically simulated for the fixed values of the parameters $\omega_0 = 0$, $\Delta = 0.05$, $\kappa_1 = -3$ and $\kappa_2 = 1$. The values of the parameter p were first increased progressively for $p_0, p_0 + \delta p, \ldots, p_0 + n\delta p$ (forward continuation) and then decreased from $p_0 + n\delta p$ to p_0 (backward continuation). For each fixed p, the stationary post-transient values of the order parameter $|R|$ were computed and depicted in Fig. 1. In this diagram, the lower branch indicates the incoherent state, when the oscillators are completely desynchronized and scattered uniformly across all phases. The upper branch represents the state in which the conformists and contrarians are partially synchronized into two diametrically opposed clusters whose phases are separated by the angle π. The forward and backward continuations lead to the sudden jumps of the order parameter from zero (incoherent state) to a finite value (coherent state) and back. The jumps take place at different values of the parameter p. The stable incoherent and coherent states coexist in the interval of p between the jumps of the order parameter.

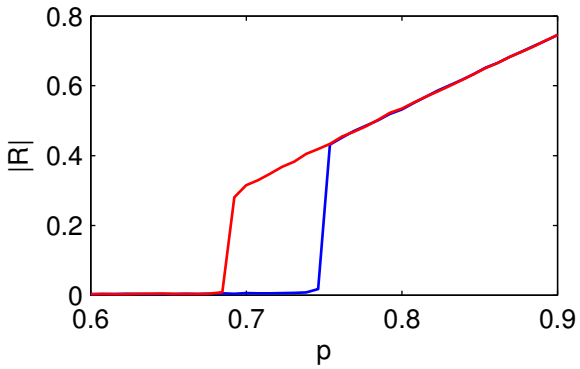

Fig. 1 Synchronization diagram for the generalized Kuramoto model (1) consisting of $N = 10000$ coupled phase oscillators at the parameter values $\omega_0 = 0$, $\Delta = 0.05$, $\kappa_1 = -3$ and $\kappa_2 = 1$. Blue (dark) and red (light) curves show the forward and backward continuations, respectively. The continuation step is $\delta p = 0.0075$ (Color figure online)

The main advantage of this model is that it admits an analytical treatment in the thermodynamic limit of infinite number of oscillators $N \to \infty$. In the next sections, we will use this approach to facilitate the analysis of our proposed bistability control algorithms.

2.2 Synaptically coupled FitzHugh-Nagumo neurons

In this section, we present a bistable network constructed in a similar way as described above, but instead of the phase oscillators as units of the network we utilize FHN [43,44] neurons. Moreover, we take into account the synaptic coupling between neurons and the presence of noise. Specifically, our model is as follows:

$$\dot{v}_j = f(v_j) - w_j + I - I_{\mathrm{syn}} - I_{\mathrm{con}} + \xi_j, \tag{5a}$$

$$\dot{w}_j = \varepsilon_j(b_0 + b_1 v - w_j) \tag{5b}$$

for $j = 1, \ldots, N$. Here the variable v_j denotes the membrane potential and w_j is the recovery variable of the jth neuron, $f(v_j) = v_j - v_j^3/3$ is the cubic source term of an ionic current and I is a constant current that defines the spiking regime of uncoupled neurons. The current I_{syn} defines the coupling between neurons and I_{con} is the control current, which will be defined in the next sections. Here we take $I_{\mathrm{con}} = 0$. The last term in Eq. (5a) is the white Gaussian noise, which is different and independent for each neuron. We assume that the mean value of the noise is zero $\langle \xi_j \rangle = 0$ and the standard deviation is $\sigma_{\xi_j} = 0.1$. The parameter ε_j defines the ratio between the characteristic time scales of v_j and w_j variables and also the spiking period of the jth neuron. To scatter the spiking periods of the neurons we choose ε_j randomly from the Gaussian distribution with the mean $\langle \varepsilon \rangle = 0.02$ and the standard deviation

$\sigma_\varepsilon = 0.1\langle\varepsilon\rangle$. The other parameters are chosen as follows $b_0 = 2$ and $b_1 = 1.5$.

To mimic realistic junctions between neurons, we couple them synaptically. We assume for simplicity that the coupling is global and write the term of synaptic current in the form

$$I_{\rm syn} = K_j(v_j - U_j)\frac{1}{N-1}\sum_{k\neq j}\Theta(v_k - v_0), \tag{6}$$

where K_j is the coupling strength and U_j defines the reversal potential of the jth neuron. $\Theta(v) = 1/[1 + \exp(-(v - v_{\rm th})/\Delta)]$ is the sigmoid function with the threshold parameter $v_{\rm th} = 1.5$ and the width $\Delta = 0.1$. In analogy to the previous model, we subdivide randomly the whole population of N neurons into two groups consisting of $N_{\rm exc}$ and $N_{\rm inh}$ neurons, characterized by the excitatory and inhibitory coupling, respectively. We distinguish them by the values of the parameters K_j and U_j. For excitatory coupled neurons, we choose $K_j = \kappa_1 = 0.4$ and $U_j = u_1 = 2.5$, while for inhibitory coupled neurons, we take $K_j = \kappa_2 = 1.2$ and $U_j = u_2 = -2.5$. We denote by $p = N_{\rm exc}/N$ the proportion of excitatory coupled neurons.

The use of the order parameter (2) as a synchronization criterion is problematic for the system (5), since it is difficult to define the phases of individual neurons when their dynamics is complex. Here we use an alternative synchronization criterion based on the variance ${\rm Var}(V)$ of the mean field:

$$V(t) = \frac{1}{N}\sum_{j=1}^{N} v_j(t). \tag{7}$$

In the synchronized state, when all neurons spike simultaneously, the value of this parameter is large, while in the incoherent state it is close to zero. In addition, we introduce the variances ${\rm Var}(V_{\rm exc})$ and ${\rm Var}(V_{\rm inh})$ for the mean fields of excitatory and inhibitory coupled neurons in order to separately measure the synchronization level in each of the subpopulations.

Figure 2 shows the dependence of the variances ${\rm Var}(V)$, ${\rm Var}(V_{\rm inh})$ and ${\rm Var}(V_{\rm exc})$ on the parameter p. The computations were performed for the total number of $N = 5000$ neurons with the continuation step $\delta p = 0.017$. The hysteresis in these dependencies indicates the presence of the bistability. In the interval of the parameter $p \in (0.45, 0.62)$ the phase space of the system has two attractors related to the coherent and incoherent states.

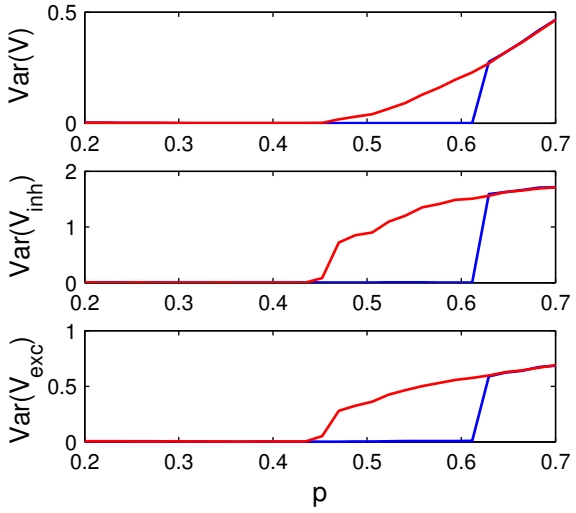

Fig. 2 Synchronization diagrams for the network of $N = 5000$ synaptically coupled FHN neurons (5). Blue (dark) and red (light) curves show the forward and backward continuations, respectively. The continuation step is $\delta p = 0.0075$, the values of other parameters are presented in the text. Equations (5) were integrated by Euler-Maruyama method with time step $h = 0.05$ (Color figure online)

2.3 Network of chaotic Rulkov neurons

Another bistable network, which will be tested by our control algorithms, is again constructed in the spirit of Ref. [37], but now we utilize Rulkov [45] neurons as units of the network. Rulkov has designed his neuron as a simple 2D map in order to model chaotic neural bursting. This model is computationally efficient for simulating very large networks of neurons. Our network constructed from Rulkov neurons reads:

$$x_j(t+1) = \frac{\alpha}{(1 + x_j^2(t))} + y_j(t) + K_j X(t) + I_{\rm con}, \tag{8a}$$

$$y_j(t+1) = y_j(t) - \mu(x_j(t) - \sigma) \tag{8b}$$

for $j = 1, \ldots, N$. Here x_j and y_j are dynamic variables of the jth Rulkov neuron and t is the discrete time. The neurons are coupled via mean field

$$X(t) = \frac{1}{N}\sum_{j=1}^{N} x_j(t). \tag{9}$$

where K_j is the coupling strength of the jth neuron and N is the total number of neurons. Again, we assume that there are two subpopulations, consisting of N_- and N_+ neurons. Each neuron in the first subpopulation is negatively coupled to the mean field with the same coupling coefficient $K_j = \kappa_1 = -0.5$, while neurons in the second population are coupled positively with $K_j = \kappa_2 = 0.25$. The last term $I_{\rm con}$ in the right hand side of Eq. (8a) represents the control current, which will be defined in Secs. 3 and 4. Here we consider the system without control, thus $I_{\rm con} = 0$. We take the values of the parameters $\alpha = 4.3$, $\mu = 0.01$, $\sigma = -1$, which correspond to a chaotic bursting regime of the

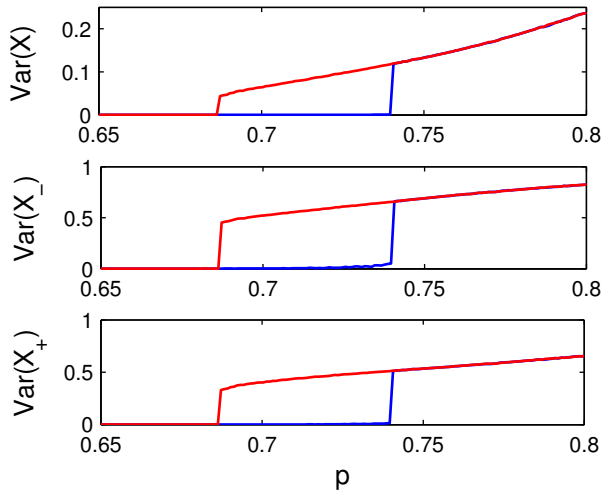

Fig. 3 Synchronization diagrams for the network of $N = 20000$ positively and negatively coupled Rulkov neurons (8). Blue (dark) and red (light) curves show the forward and backward continuations, respectively. The continuation step is $\delta p = 0.001$, the values of other parameters are presented in the text (Color figure online)

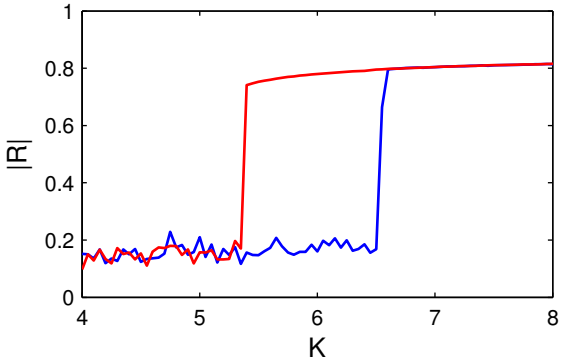

Fig. 4 Synchronization diagram for the scale-free network of $N = 1000$ phase oscillators (10). The adjacency matrix is generated using the configuration model [46] with the parameters $\gamma = 2.4$, $\langle k \rangle = 6$ and $k_{\min} = 1$. The natural frequency for each oscillator is equal to its degree, $\omega_j = k_j$. Blue (dark) and red (light) curves show the forward and backward continuations, respectively. The continuation step is $\delta K = 0.05$ (Color figure online)

isolated Rulkov neurons. Note that in our constructed network all neurons are identical, however, we assign them different initial conditions.

We characterize the coherence of the network as above by estimating the variance of the total mean field $\mathrm{Var}(X)$ and the variances of the mean fields of the negatively and positively coupled subpopulations, $\mathrm{Var}(X_-)$ and $\mathrm{Var}(X_+)$, respectively. The dependencies of these parameters on the the proportion of positively coupled neurons $p = N_+/N$ for $N = 20000$ are shown in Fig. 3. We see that the coherent and incoherent attractors coexist for $p \in (0.69, 0.74)$.

2.4 Scale-free network of phase oscillators

The last bistable network analyzed in this paper differs essentially from the previous three by the topology of connections. Now we consider a network of phase oscillators connected by a scale-free topology:

$$\dot{\theta}_j = \omega_j + K \sum_{l=1}^{N} a_{jl} \sin(\theta_l - \theta_j). \qquad (10)$$

Here a_{jl} is an element of the adjacency matrix $\mathbf{A}$, which encodes network's topology. For the connected j and l oscillators, the matrix element is equal to one, $a_{jl} = 1$, while $a_{jl} = 0$ otherwise. We assume that the coupling is symmetric $a_{lj} = a_{jl}$ and there are no self-connections $a_{ll} = 0$. In the scale-free networks, the proportion $P(k)$ of nodes having k connections satisfies for large k the power law $P(k) \sim k^{-\gamma}$ with $\gamma > 0$. It was shown [39] that in scale free networks the hysteresis appears when the natural frequencies ω_j of oscillators are positively correlated with their degrees (numbers of connections k_j), i.e. when $\omega_j \sim k_j$.

We quantify the degree of synchronization among oscillators by the order parameter (2). Figure 4 shows the dependence of this parameter on the coupling strength K for a scale-free network consisting of $N = 1000$ oscillators. The adjacency matrix was generated according to the configuration model [46] with the scale factor $\gamma = 2.4$, average degree $\langle k \rangle = 6$ and minimal junction number $k_{\min} = 1$. The natural frequency of each oscillator were chosen equal to its degree, $\omega_j = k_j$. The observed hysteresis indicates the bistability of synchronization in the interval of the coupling strength $K \in (0.54, 0.65)$.

3 Eliminating synchronization via an act-and-wait algorithm

As a first candidate for controlling synchronization in bistable networks, we consider the algorithm, which in control theory is known as an act-and-wait control method [30–33]. Recently we have applied this algorithm to monostable oscillatory networks, which possess stable coherent and unstable incoherent states, and shown that it can effectively stabilize the incoherent state [20]. Now we verify the capability of this algorithm to switch a bistable network from the stable coherent state to the stable incoherent state.

As applied to neural networks, the act-and-wait algorithm is formulated as follows (see [20] for details). It

is assumed that only mean field of the network is available for observation and only homogeneous perturbations are allowed. The latter condition means that all units of the network can be acted only equally. These assumptions allow us to implement the method with a single electrode. The algorithm involves the periodic repetition of two stages. In the first (wait) stage, the mean field of the control-free population is registered and recorded in a memory, and in the second (act) stage, the memorized signal is fed back to the system. In fact, this algorithm utilizes a time-delayed feedback with the periodically switched on and off feedback gain. The control force is proportional to the product of the mean field delayed by a period τ_w and the T_c-periodic act-and-wait switching function

$$G(t) = \begin{cases} 0, & 0 \le t < \tau_w \\ 1, & \tau_w \le t < \tau_w + \tau_a = T_c, \end{cases} \tag{11}$$

where τ_a and τ_w are the durations of act and wait stages, respectively. For real neural networks it is important to avoid an overlap of the registration and stimulation processes, since the stimulation current typically exceeds the measured neuronal current by several orders of magnitude and reliable registration of neuronal activity in the presence of simultaneous stimulation is impossible [47]. In order to ensure that the stimulation is performed by a signal registered from the control-free system, we have to require that the act period is less or equal to the wait period $\tau_a \le \tau_w$. The latter inequality is superior from the mathematical point of view as well, since it allows us to treat the controlled system as a finite-dimensional one, despite the fact that the time-delayed feedback is usually associated with an infinite-dimensional phase space [30–32, 20]. In this paper, we restrict ourselves to the case of equal act and wait durations $\tau_w = \tau_a \equiv \tau$. Then the period of act-and-wait switching is $T_c = 2\tau$ and the 2τ-periodic function (11) can be presented as

$$G(t) = H\left[-\sin(\pi t/\tau)\right], \tag{12}$$

where $H(\cdot)$ is the Heaviside step function.

In what follows, we verify the efficacy of the act-and-wait algorithm for eliminating synchronization in bistable networks described above (see Sec. 2). We present the results only for the first three models. The last model is omitted, since it turned out that this algorithm is inefficient for the scale-free networks. Nonetheless, in Sec. 4 we will show that the bistable scale-free networks can be effectively controlled by the MCR algorithm.

3.1 Kuramoto model with positive and negative couplings

In the presence of the act-and-wait control, the Kuramoto model Eqs. (3) transform to

$$\dot\theta_j = \omega_j + \mathrm{Im}\left[(K_j R - PG(t)R_\tau)\, e^{-i\theta_j}\right] \tag{13}$$

for $j = 1, \dots, N$. Here the additional term $PG(t)R_\tau$ stands for the act-and-wait control force, where P is the feedback strength, $G(t)$ is the periodic function defined by Eq. (12) and the subscript τ in R_τ denotes the time-delayed value $R_\tau \equiv R(t-\tau)$. The form of the control term is derived from a model of coupled and stimulated Stuart-Landau oscillators in the assumption that only mean field is available for the measurement and the control perturbation is applied homogeneously (cf. Ref. [20]).

The results of successful elimination of synchronization in system (13) consisting of $N_- = 1500$ contrarians and $N_+ = 3500$ conformists are presented in Fig. 5. The blue (dark) curve in panel (a) shows the dynamics of the order parameter (2). For $t < 100$, the control perturbation is off, P=0. The initial conditions are chosen such that the bistable system settles to the synchronized state. In this state, the order parameter fluctuates around the value $|R| = 0.31$. The contrarians and conformists crowd into two diametrically opposed clusters whose phases are separated by the angle π. This is evident from the dynamics of the phase distribution shown in panel (b). For $100 < t < 200$, the act-and-wait control algorithm with the strength $P = 2$ is activated. We see that the act-and-wait feedback perturbation destroys the coherent clustered state. However, the feedback perturbation is constructed in such a way that it does not destroy the incoherent state of the system, and what is more this state remains stable in the presence of control. The feedback seemingly makes the incoherent state the only attractor of the system and because of that it settles to this state after a short transient period. As a result the value of the order parameter falls to zero and the phase distribution becomes uniform. For $t > 200$, the control force is switched off, $P = 0$. Since the control-free system is bistable, it remains in its stable incoherent state in the absence of control.

The system (13) admits an analytical treatment and essential simplification in the thermodynamic limit of infinite number of oscillators, $N \to +\infty$. Using the Ott-Antonsen ansatz [48] with the assumption that the natural frequencies ω_j satisfy the Lorentz distribution (4), system (13) can be reduced to only two differential equations (cf. [37,20]):

$$\dot r_1 = \kappa_1(R^* - Rr_1^2)/2 - (i\omega_0 - \Delta)r_1 + F_1, \tag{14a}$$

$$\dot r_2 = \kappa_2(R^* - Rr_2^2)/2 - (i\omega_0 - \Delta)r_2 + F_2, \tag{14b}$$

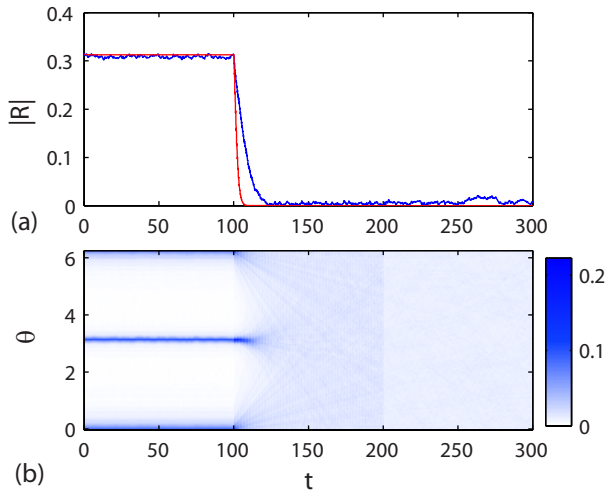

Fig. 5 Elimination of synchronization by act-and-wait control in the Kuramoto model (13) for $N = 5000$, $p = 0.7$, $\omega_0 = 0$, $\Delta = 0.05$, $\kappa_1 = -3$ and $\kappa_2 = 1$. For $t < 100$, the system is control-free ($P = 0$), in the interval $100 < t < 200$ the act-and-wait control is on with $P = 2$ and $\tau = 0.2$ and for $t > 200$, the system is again control-free. (a) Blue (dark) curve shows the absolute value of the order parameter computed from the system (13) while red (light) curve shows the same result obtained from the reduced system (14). (b) Dynamics of the phase distribution of Eqs. (13). The values of the phase density are encoded by colors (Color figure online)

where r_1 and r_2 are the complex order parameters of the contrarian and conformist subpopulations, respectively and

$$F_{1,2} = -PG(t)(R^*_\tau - R_\tau r^2_{1,2})/2 \tag{15}$$

are the act-and-wait feedback forces. The total order parameter (2) is related to this parameters via a simple algebraic expression

$$R = (1-p)r^*_1 + pr^*_2. \tag{16}$$

To verify the validity of the reduced system (14), we have computed the dynamics of the order parameter using Eqs. (14) with the same conditions as above. The result is depicted in Fig. 5 (a) by the red (light) curve. We see that this curve is close to the blue (dark) curve obtained by direct simulation of the original system (13).

The reduced system (14) is computationally much more efficient than the original system (13) and can be used to investigate the performance of the act-and-wait algorithm in more details. In Fig. (6) we show how the control performance depends on the choice of the coupling strength P and the delay time τ. For a given pair of the parameters (P, τ), we took the initial conditions at the synchronized state and applied for some period of time the act-and-wait control. Then we switched off the

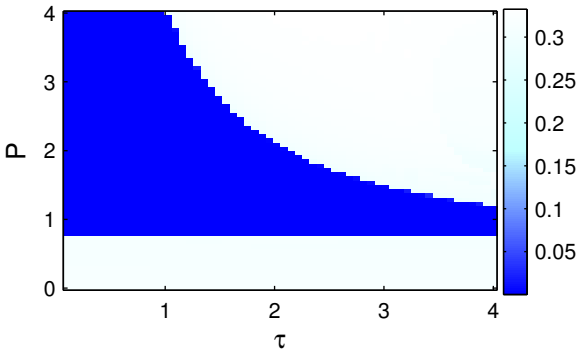

Fig. 6 Domain of successful elimination of synchronization in the plain of parameters (P, τ) for the Kuramoto model with positive and negative couplings estimated from the reduced system (14). The mean absolute values of the order parameter computed after application of act-and-wait control are encoded by colors. The values of the parameters are the same as in Fig. 5 (Color figure online)

control and computed the mean absolute value of the order parameter in the post transient regime. These values encoded by colors are depicted in the plane (P, τ) in Fig. (6). In this figure, the colored region corresponds to the domain of successful control. We see that the increase of the delay τ narrows the range of the strength P where the act-and-wait control is effective. Also, the increase of the strength P narrows the range of τ where the elimination of synchronization is successful.

3.2 Synaptically coupled FitzHugh-Nagumo neurons

The act-and-wait control algorithm works well for rather complicated systems. Here we show that it can eliminate synchronization in a noisy system of synaptically coupled FHN neurons introduced in Sec. 2.2. Assuming that only the mean field is available for the measurement and only homogeneous perturbations are allowed, the control current in the model (5) can be written as

$$I_{\rm con}(t) = G(t)PV(t-\tau), \tag{17}$$

where $G(t)$ is the periodic function (12), P is the feedback strength and $V(t-\tau)$ is a time-delayed value of the mean field (7).

Figure 7 demonstrates the results of successful elimination of synchronization in the network (5) consisting of $N = 5000$ neurons, a half of which is coupled inhibitory and another half is coupled excitatory. We show the dynamics of the mean fields $V(t)$, $V_{\rm inh}(t)$ and $V_{\rm exc}(t)$. Without control ($t < 2000$), the network is in the synchronized state; here all mean fields exhibit almost periodic oscillations with large amplitude. In the time interval $2000 < t < 5000$, the act-and-wait control

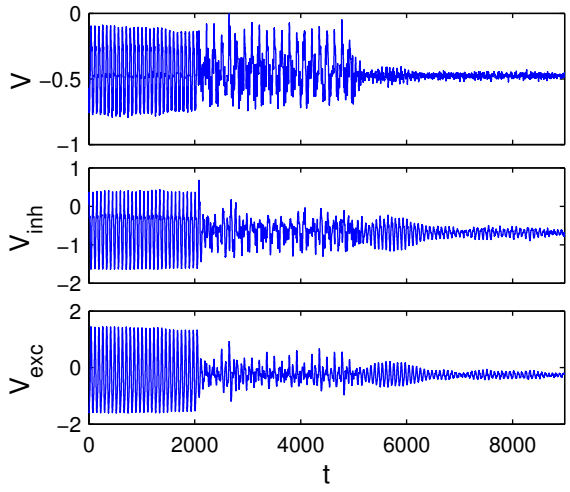

Fig. 7 Elimination of synchronization by act-and-wait control in the network of synaptically coupled FHN neurons (5) for $N = 5000$ and $p = 0.5$. V denotes the mean field of the whole population, while V_{inh} and V_{exc} are the mean fields of inhibitory and excitatory coupled subpopulations. For $t < 2000$, the system is control-free ($P = 0$), in the interval $2000 < t < 5000$, the act-and-wait control is on with $P = 0.2$ and $\tau = 71$ and for $t > 5000$, the system is again control-free

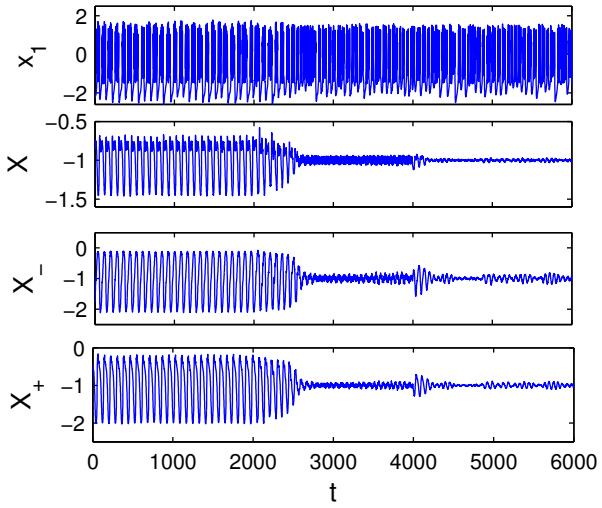

Fig. 8 Elimination of synchronization by act-and-wait control in the network of chaotic Rulkov neurons for $N = 20000$ and $p = 0.7$. The panels show, from top to bottom, the dynamics of the unit x_1, and of the mean fields X, X_- and X_+. For $t < 2000$, the system is control-free ($P = 0$), in the interval $2000 \le t \le 4000$ the act-and-wait control is on with $P = 0.025$ and $\tau = 7$ and for $t > 4000$, the system is again control-free

is activated with the strength $P = 0.2$ and the delay time $\tau = 71$, chosen close the period of oscillations of the mean field of control-free system. We see that the control decreases the amplitudes of variations of the mean fields. For $t > 5000$, the control is switched off and the system settles to the stable incoherent state. Note that the amplitudes of oscillations are higher during the control than after the control is turned off. This means that at the end of the control the system state does not reside exactly in the incoherent attractor, but it enters its basin of attraction.

3.3 Network of chaotic Rulkov neurons

As a last example demonstrating the efficacy of the act-and-wait control algorithm, we consider elimination of synchronization in the network of chaotic Rulkov neurons (8). Here we take the same form of the control current as in the network of FHN neurons

$$I_{\text{con}}(t) = G(t)PX(t-\tau) \tag{18}$$

with the only difference that the time t and the delay time τ are now discrete.

The results of successful elimination of synchronization for the network consisting of $N_+ = 14000$ positively and $N_- = 6000$ negatively coupled neurons are presented in Fig. 8. We show the dynamics of the unit $x_1(t)$ as well as of the mean fields $X(t)$, $X_-(t)$ and $X_+(t)$. For time $t < 2000$, the control is off and the system is in synchronized state. Here the individual neurons display chaotic bursting (the top panel), while the mean fields show rather regular low-frequency oscillations with a large amplitude. When the act-and-wait control is activated ($2000 \le t \le 4000$), the amplitudes of the mean fields quickly decay, while the dynamics of individual units little change. The individual neurons do not produce macroscopic oscillation since they burst incoherently. After switching off the control ($t > 4000$) the system remains in the incoherent state.

4 Eliminating synchronization via a multisite coordinated reset stimulation

The MCR stimulation was introduced in Ref. [13] as a nonfeedback algorithm for suppression synchronization in monostable neural networks that possess a stable coherent and an unstable incoherent state. Here we test the ability of this algorithm to eliminate synchronization in bistable oscillatory networks.

Unlike to the act-and-wait control algorithm, the MCR stimulation uses inhomogeneous perturbations and in neural networks is implemented by means of several electrodes, which can act independently on different sites of neural population. The main idea behind the method is to apply to the electrodes periodic signals with shifted phases. When there are M electrodes the phase shifts are uniformly distributed in the

interval $(0; 2\pi)$ with the step $2\pi/M$. In this way, the electrodes entrain subpopulations of neurons, so that M synchronous clusters are formed. When the stimulation is switched off, the clusters desynchronize. After some time the population synchronizes to the one-cluster states again, and stimulation should be switched on again, and so forth. Since the method is nonfeedback it cannot hold a monostable network exactly in its unstable incoherent state, but by periodic switching on and off the stimulation one can partially suppress the synchronization.

When controlling the bistable networks by MCR algorithm, we do not need to periodically switch on and off the stimulation. Below we show that synchronization can be eliminated by only single switched on and off cycle. Note that the coordinated reset may be achieved by means of a high-frequency pulse train [13] or using a soft stimulation [12] with the frequency close to the mean frequency of the network. Here we use the latter approach.

The MCR stimulation is robust against variations of model parameters and is insensitive to the specific topology of the network. Among others, here we show that it works well for a bistable scale-free network.

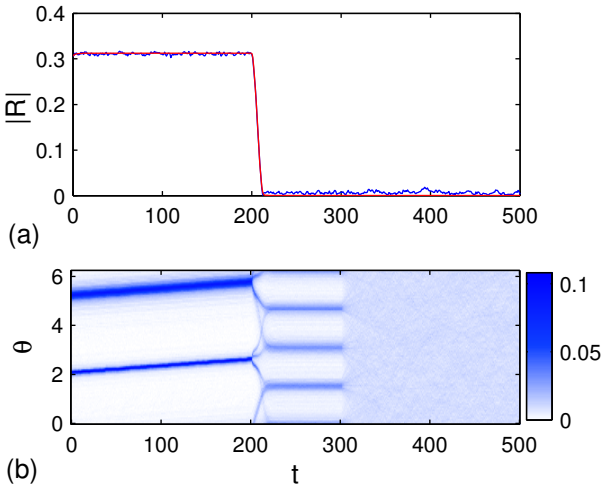

Fig. 9 Elimination of synchronization by MCR stimulation in the Kuramoto model (19) for $N = 5000$, $p = 0.7$, $\omega_0 = 0$, $\Delta = 0.05$, $\kappa_1 = -3$ and $\kappa_2 = 1$. For $t < 200$, the system is control-free ($a = 0$), in the interval $200 < t < 300$ the MCR stimulation is on with $M = 2$, $a = 0.3$ and $\Omega = 0$ and for $t > 300$, the system is again control-free. (a) Blue (dark) curve shows the absolute value of the order parameter computed from the system (19) while red (light) curve shows the same result obtained from the reduced system (20). (b) Dynamics of the phase distribution of Eqs. (19) (Color figure online)

4.1 Kuramoto model with positive and negative couplings

First we verify the performance of the MCR stimulation algorithm for the Kuramoto model (3). In the presence of the MCR stimulation this model reads:

$$\dot{\theta}_j = \omega_j + \mathrm{Im}\left[\left(K_j R + a e^{i(\Omega t + \phi_j^{(m)})}\right) e^{-i\theta_j}\right] \qquad (19)$$

for $j = 1, \ldots, N$. Here the amplitude a and the frequency Ω of the MCR stimulation are equal for all units of the network, while the phases $\phi_j^{(m)}$ are different. We assume that in the case of M electrodes, each of them stimulates independently N/M different units of the network. The phase shifts of periodic signals applied to the electrodes are chosen as $2\pi(m-1)/M$, where $m = 1, \ldots, M$ is the number of the electrode. In this way the whole population is split into M distinct clusters related to the different stimulation sites, respectively. For all oscillatory units with the index j belonging to the mth cluster, the stimulation phase is $\phi_j^{(m)} = 2\pi(m-1)/M$. In our numerical simulations, the units are randomly assigned to the different clusters.

We tested the MCR stimulation algorithm with $M = 4$ for the network (19) consisting of $N_- = 1500$ contrarians and $N_+ = 3500$ conformists. In Fig. 9, the panels (a) and (b) show the dynamics of the order parameter (2) and of the phase distribution, respectively. For $t < 200$, the control-free system is in the synchronized regime in which contrarians and conformists are crowded into two opposed clusters. For $200 < t < 300$, the MCR stimulation is switched on and the network resynchronizes according to the applied signals so that that phases of the oscillators are spread into new four uniformly distributed clusters separated by the angle $\pi/2$ with equal proportion of the oscillators in each cluster. Note that the contrarian and conformist oscillators are now mixed in each of the clusters. The state resulting from the MCR stimulation has more uniform phase distribution as compared to the initial synchronized state and thus it should be closer to the incorrect state in the phase space of the free system, since the latter is characterized by the uniform distribution of phases. This explains why the state resulting from the MCR stimulation appearers to lie in the basin of attraction of the incoherent attractor of the free system and why the system approaches this attractor when the stimulation is switched off ($t > 300$). We see that after a short transient period the phase distribution becomes totally uniform and the order parameter almost vanishes.

In the thermodynamic limit $N \to \infty$, the Kuramoto model (19) under MCR stimulation can be reduced by Ott–Antonsen ansatz [48] to only $2M$ differential equa-

tions:

$$\dot{r}_{1,m} = \frac{\kappa_1}{2}(R^* - Rr_{1,m}^2) - (i\omega_0 - \Delta)r_{1,m} + \bar{F}_1^{(m)}, \quad (20a)$$

$$\dot{r}_{2,m} = \frac{\kappa_2}{2}(R^* - Rr_{2,m}^2) - (i\omega_0 - \Delta)r_{2,m} + \bar{F}_2^{(m)} \quad (20b)$$

for $m = 1, \ldots, M$. Here $r_{1,m}$ and $r_{2,m}$ are the complex order parameters of the contrarian and conformist subpopulations, respectively, which are stimulated with the periodic signal having phase shift $\phi^{(m)} = 2\pi(m-1)/M$. The stimulation force in system (20) reads:

$$\bar{F}_j^{(m)} = -\frac{a}{2}\left(e^{-i(\Omega t+\phi^{(m)})}r_{j,m}^2 - e^{i(\Omega t+\phi^{(m)})}\right) \quad (21)$$

for $j = 1, 2$ and $m = 1, \ldots, M$. The order parameter of the whole network can be computed as

$$R = \sum_{m=1}^{M}\{(1-p)r_{1,m}^* + pr_{2,m}^*\}. \quad (22)$$

In Fig. 9 (a), we compare the dynamics of the absolute value of the order parameter computed from the reduced system (20) (red/light curve) with that obtained by direct simulation of the original system (19) (blue/dark curve). The good coincidence of the above results means that the reduced system approximates well the dynamics of large networks of the Kuramoto oscillators in the presence of MCR stimulation.

4.2 Synaptically coupled FitzHugh-Nagumo neurons

The MCR stimulation current in the model (5) of synaptically coupled FHN neurons has the form

$$I_{\text{con}}(t) = a\cos(\Omega t + \phi_j^{(m)}), \quad (23)$$

where $\phi_j^{(m)} = 2\pi(m-1)/M$ is the phase of the stimulation signal coming from the m th electrode to the jth neuron. The results of successful elimination of synchronization in the network (5) consisting of $N = 5000$ neurons are presented in Fig. 10. The algorithm works well, although here we used only two ($M = 2$) stimulation electrodes.

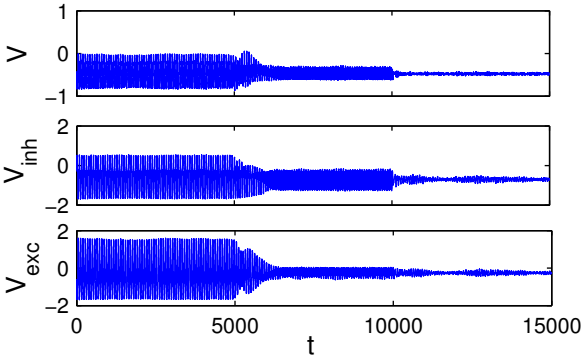

Fig. 10 Elimination of synchronization by MCR stimulation in the network of synaptically coupled FHN neurons (5). The parameters of the network are the same as in Fig. 7. For $t < 5000$, the system is control-free ($a = 0$), in the interval $5000 < t < 10000$ the MCR stimulation is on with $M = 2$, $a = 0.1$ and $\Omega = 2\pi/74$ and for $t > 10000$, the system is again control-free

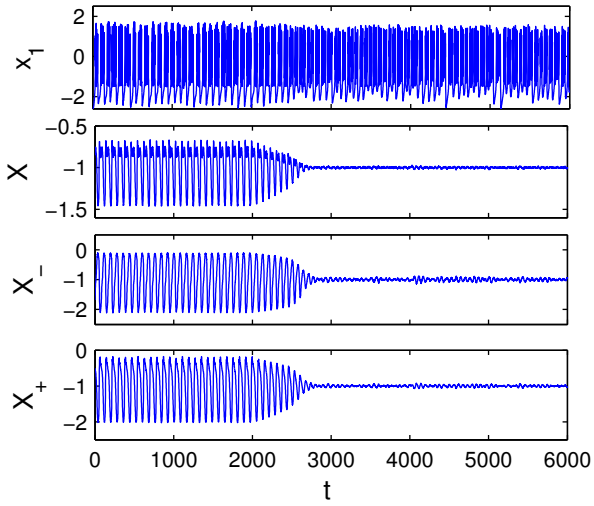

Fig. 11 Elimination of synchronization by MCR stimulation in the network of chaotic Rulkov neurons for $N = 30000$ and $p = 0.7$. For $t < 2000$, the system is control-free ($a = 0$), in the interval $2000 \le t \le 4000$ the MCR stimulation with $M = 3$, $a = 0.02$ and $\Omega = 2\pi/60$ is switched on and for $t > 4000$, the system is again control-free

4.3 Network of chaotic Rulkov neurons

For the network of chaotic Rulkov neurons (8), we use the same form of the control current as for the network of FHN neurons

$$I_{\text{con}}(t) = a\cos(\Omega t + \phi_j^{(m)}) \quad (24)$$

with the only difference that the time t is now a discrete variable. In Fig. 11 we demonstrate an example of successful elimination of synchronization in the network consisting of $N = 30000$ neurons. We used the MCR algorithm with three ($M = 3$) stimulation electrodes. As well as in Fig. 8, we show the dynamics of four parameters $x_1(t)$, $X(t)$, $X_-(t)$ and $X_+(t)$. For $t < 2000$, the control-free system is in synchronized regime. For $2000 \le t \le 4000$, the MCR stimulation is activated and then for $t > 4000$ it is switched off. As a result, the network settles to the stable incoherent state where only small fluctuations of the mean fields $X(t)$, $X_-(t)$ and $X_+(t)$ are observed.

4.4 Scale-free network of phase oscillators

The MCR stimulation approach goes beyond the model of globally coupled populations and admits some spatial structure of the network. Here we demonstrate its efficacy to eliminate synchronization in the scale-free network (10). To this end, we add to the Eqs. (10) the MCR stimulation term of the same form as for the Kuramoto model with positive and negative couplings (see Eqs. (19)):

$$\dot{\theta}_j = \omega_j + K\sum_{l=1}^{N} a_{jl}\sin(\theta_l - \theta_j) + a\sin(\Omega t + \phi_j^{(m)} - \theta_j) \tag{25}$$

The results of numerical simulation of the network (25) are presented in Fig. 12. The coupling strength K is chosen equal to 6 and the other parameters of the network are the same as in Sec. 2.4. The panel (a) shows the dynamics of the order parameter, while the panel (b) displays an evolution of the phase distribution. For $t < 40$, the control-free network is in the synchronized state, then for $40 < t < 50$, the MCR stimulation with $M = 4$, $a = 10$ and $\Omega = 2\pi$ is switched on, and for $t > 50$ it is switched off. As a result the system settles to the stable incoherent state. The success of control can be again explained by the fact that the MCR stimulation produces the state with rather uniform phase distribution, which falls within the basin of attraction of the incoherent attractor of the free system.

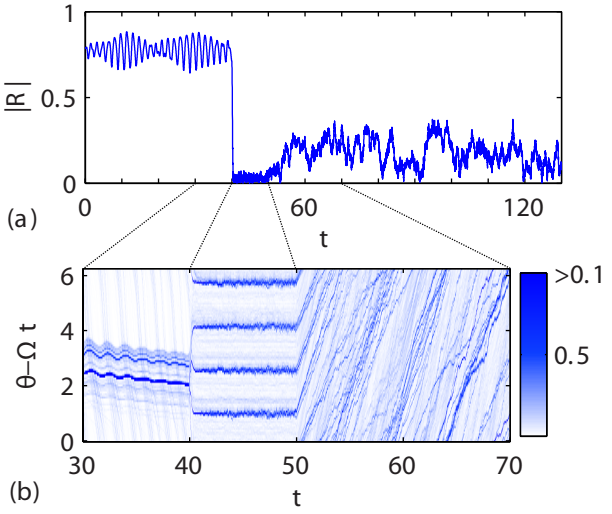

Fig. 12 Elimination of synchronization by MCR stimulation in the scale free network (25) consisting of $N = 1000$ oscillators with coupling strength $K = 6$. Other parameters of the network are the same as in Fig. 4. For $t < 40$, the system is control-free ($a = 0$), in the interval $40 < t < 50$ the MCR stimulation is on with $M = 4$, $a = 10$ and $\Omega = 2\pi$, and for $t > 300$, the system is again control-free. (a) Dynamics of the absolute value of the order parameter. (b) Evolution of the phase distribution of Eqs. (25). Note different scales of time in panels (a) and (b) (Color figure online)

5 Conclusions

In this paper, the problem of controlling synchronization in bistable oscillatory networks has been considered. We have shown that the bistability effect is characteristic not only for the Kuramoto-type models, but also for a network of chaotic Rulkov neurons connected through the mean field with positive and negative coupling coefficients as well as for a stochastic model of synaptically all-to-all coupled FitzHugh-Nagumo neurons with excitatory and inhibitory interaction. All these systems have coexisting stable coherent and incoherent states in a certain range of parameters. In order to switch a bistable network from the stable coherent state to the stable incoherent state, we have suggested and tested two different algorithms. Both of them take into account constraints typical for real-world neural networks; they satisfy the requirement that the control and measurements of the system are available only on a macroscopic level.

The first, act-and-wait control algorithm, is based on periodic repetition of two stages. In the first stage, the mean field of the free system is measured and recorded, while in the second stage, all units of the network are homogeneously forced by the recorded signal. In fact, this algorithm uses a time delayed feedback with periodically switched on and off feedback gain. The feedback is constructed in such a way that it preserves the stable incoherent state of the system but destroys its coherent state. We have shown that this algorithm is efficient for networks with all-to-all coupling topology. The advantage of this algorithm is that it can be implemented in neural networks by a single electrode.

The second algorithm is based on multisite coordinated reset stimulation. This algorithm is nonfeedback and does not require online measurements of the system state. However, the algorithm uses inhomogeneous perturbations and its implementation requires several electrodes. Different sites of the network are stimulated through the electrodes by periodic signals with shifted phases. As a result a multicluster synchronous state with uniformly scattered phases is formed. We have shown by examples that such a state lies in the basin of attraction of the incoherent attractor of the free system, so that after switching off the stimulation the network approaches the incoherent state. The main advantage of this approach is that it works well not only for networks with all-to-all coupling topology but is applicable for

more complex networks as well. We have demonstrated its capability to eliminate synchronization in a bistable network with a nontrivial scale-free topology.

Acknowledgements This work is supported by grant No. MIP-15040/2015 of the Research Council of Lithuania.

References

1. Kuramoto, Y.: Chemical Oscillations, Waves and Turbulence. Springer, New York (1984)
2. Pikovsky, A., Rosenblum, M., Kurths, J.: Synchronization. A universal concept in nonlinear sciences. Cambridge university press (2001)
3. Mosekilde, E., Maistrenko, Y., Postnov, D.: Chaotic synchronization applications to living systems. World Scientific (2002)
4. Arenas, A., Díaz-Guilera, A., Kurths, J., Moreno, Y., Zhou, C.: Synchronization in complex networks. Physics Reports **469**(3), 93 – 153 (2008)
5. Strogatz, S.H., Abrams, D.M., McRobie, A., Eckhardt, B., Ott, E.: Crowd synchrony on the Millennium Bridge. Nature **438**, 43–44 (2005)
6. Izhikevich, E.M.: Dynamical Systems in Neuroscience: The Geometry of Excitability and Bursting. The MIT Press (2007)
7. Schnitzler, A., Gross, J.: Normal and pathological oscillatory communication in the brain. Nat. Rev. Neurosci. **6**, 285–296 (2005)
8. Alberts, W.W., Wright, E.W., Feinstein, B.: Cortical potentials and Parkinsonian tremor. Nature **221**, 670–672 (1969)
9. Lenz, F.A., Kwan, H.C., Martin, R.L., Tasker, R.R., Dostrovsky, J.O., Lenz, Y.E.: Single unit analysis of the human ventral thalamic nuclear group tremor-related activity in functional indentified cells. Brain **117**, 531–543 (1994)
10. Goldberg, J.A., Rokni, U., Boraud, T., Vaadia, E., Bergman, H.: Spike synchronization in the cortex-basal ganglia networks of Parkinsonian primates reflects global dynamics of the local field potentials. The journal of Neuroscience **24**, 6003–6010 (2004)
11. Lytton, W.W.: Computer modelling of epilepsy. Nat Rev Neurosci **9**, 626–637 (2008)
12. Tass, P.A.: Desynchronization of brain rhythms with soft phase-resetting techniques. Biological Cybernetics **87**(2), 102–115 (2002)
13. Tass, P.A.: A model of desynchronizing deep brain stimulation with a demand-controlled coordinated reset of neural subpopulations. Biol. Cybern. **89**, 81–88 (2003)
14. Popovych, O.V., Tass, P.A.: Control of abnormal synchronization in neurological disorders. Frontiers in Neurology **5**(268), 1–12 (2014)
15. Rosenblum, M.G., Pikovsky, A.S.: Controlling synchronization in an ensemble of globally coupled oscillators. Phys. Rev. Lett. **92**, 114,102 (2004)
16. Rosenblum, M.G., Pikovsky, A.S.: Delayed feedback control of collective synchrony: An approach to suppression of pathological brain rhythms. Phys. Rev. E **70**, 041,904 (2004)
17. Hauptmann, C., Popovych, O., Tass, P.A.: Delayed feedback control of synchronization in locally coupled neuronal networks. Neurocomputing **65-66**, 759–767 (2005)
18. Hauptmann, C., Popovych, O., Tass, P.A.: Effectively desynchronizing deep brain stimulation based on a coordinated delayed feedback stimulation via several sites: a computational study. Biol. Cybern. **93**, 463–470 (2005)
19. Batista, C.A.S., Lopes, S.R., Viana, R.L., Batista, A.M.: Delayed feedback control of bursting synchronization in a scale-free neuronal network. Neural Networks **23**, 114–124 (2010)
20. Ratas, I., Pyragas, K.: Controlling synchrony in oscillatory networks via an act-and-wait algorithm. Phys. Rev. E **90**, 032,914 (2014)
21. Popovych, O.V., Hauptmann, C., Tass, P.A.: Effective desynchronization by nonlinear delayed feedback. Phys. Rev. Lett. **94**, 164,102 (2005)
22. Popovych, O.V., Hauptmann, C., Tass, P.A.: Control of neuronal synchrony by nonlinear delayed feedback. Biol. Cybern. **95**, 69–85 (2006)
23. Popovych, O.V., Tass, P.A.: Synchronization control of interacting oscillatory ensembles by mixed nonlinear delayed feedback. Phys. Rev. E **82**, 026,204 (2010)
24. Tukhlina, N., Rosenblum, M., Pikovsky, A., Kurths, J.: Feedback suppression of neural synchrony by vanishing stimulation. Phys. Rev. E **75**, 011,918 (2007)
25. Pyragas, K., Popovich, O., Tass, P.: Controlling synchrony in oscillatory networks with separate stimulation – registration setup. Europhys. Lett. **80**, 40,002 (2007)
26. Ming, L., Yongjun, W., Peng, J.: Washout filter aided mean field feedback desynchronization in an ensemble of globally coupled neural oscillators. Biol. Cybern. **101**, 214–246 (2009)
27. Berényi, A., Belluscio, M., Mao, D., Buzsáki, G.: Closed-loop control of epilepsy by transcranial electrical stimulation. Science **337**, 735–737 (2012)
28. Louzada, V.H.P., Araújo, N.A.M., Andrade Jr., J.S., Herrmann, H.J.: How to suppress undesired synchronization. Scientific Reports **2**, 658 (2012)
29. Pisarchik, A.N., Feudel, U.: Control of multistability. Phys. Rep. **540**, 167–218 (2014)
30. Insperger, T.: Act-and-wait concept for continuous-time control systems with feedback delay. IEEE Transactions on Control Systems Technology **14**, 974 – 977 (2006)
31. Stépán, G., Insperger, T.: Stability of time-periodic and delayed systems — a route to act-and-wait control. Annual Reviews in Control **30**, 159–168 (2006)
32. Gawthrop, P.: Act-and-wait and intermittent control: Some comments. IEEE Transactions on Control Systems Technology **18**, 1195–1198 (2010)
33. Li, B., Song, X., Zhao, J.: Act-and-wait control theory for continuous-time systems with random feedback delays. Nonlinear Dynamics and Systems Theory **13**, 171–178 (2013)
34. Martens, E.A., Barreto, E., Stogatz, S.H., Ott, E., So, P., Antonsen, T.M.: Exact results for the Kuramoto model with a bimodal frequency distribution. Phys. Rev. E **79**, 026,204 (2009)
35. Pazó, D., Montbrió, E.: Existence of hysteresis in the kuramoto model with bimodal frequency distributions. Phys. Rev. E **80**, 046,215 (2009)
36. Taylor, D., Ott, E., Restrepo, J.G.: Spontaneous synchronization of coupled oscillator systems with frequency adaptation. Phys. Rev. E **81**, 046,214 (2010)
37. Hong, H., Stogatz, S.H.: Kuramoto model of coupled oscillators with positive and negative coupling parameters: An example of conformist and contrarian oscillators. Phys. Rev. Lett. **106**, 054,102 (2011)
38. Omel'chenko, O.E., Wolfrum, M.: Nonuniversal transitions to synchrony in the Sakaguchi-Kuramoto model. Phys. Rev. Lett. **109**, 164,101 (2012)

39. Gómez-Gardeñes, J., Gómez, S., Arenas, A., Moreno, Y.: Explosive synchronization transitions in scale-free networks. Phys. Rev. Lett. **106**, 128,701 (2011)
40. Zhang, X., Hu, X., Kurths, J., Liu, Z.: Explosive synchronization in a general complex network. Phys. Rev. E **88**, 010,802 (2013)
41. Chen, H., He, G., Huang, F., Shen, C., Hou, Z.: Explosive synchronization transitions in complex neural networks. Chaos: An Interdisciplinary Journal of Nonlinear Science **23**(3), 033124 (2013)
42. Leyva, I., Sevilla-Escoboza, R., Buldú, J.M., Sendiña Nadal, I., Gómez-Gardeñes, J., Arenas, A., Moreno, Y., Gómez, S., Jaimes-Reátegui, R., Boccaletti, S.: Explosive first-order transition to synchrony in networked chaotic oscillators. Phys. Rev. Lett. **108**, 168,702 (2012)
43. FitzHugh, R.A.: Impulses and physiological states in theoretical models of nerve membrane. Biophys. J. **1**, 445–466 (1961)
44. Nagumo, J., Arimoto, S., Yoshizawa, S.: An active pulse transmission line simulating nerve axon. Proc IRE **50**, 2061–2070 (1962)
45. Rulkov, N.F.: Regularization of synchronized chaotic bursts. Phys. Rev. Lett. **86**, 183–186 (2001)
46. Newman, M.: Networks: An introduction. Oxford university press (2010)
47. Beurrier, C., Garcia, L., Bioulac, B., Hammond, C.: Subthalamic nucleus: A clock inside basal ganglia? Thalamus Relat Syst. **2**, 1–8 (2002)
48. Ott, E., Antonsen, T.M.: Low dimensional behavior of large systems of globally coupled oscillators. Chaos **18**, 037,113 (2008)